Article

A Comprehensive Recovery Process for Selective Separation and Enrichment of Copper, Zinc and Iron Minerals from a Polymetallic Ore and the Adsorption Mechanism of Collector Z-200

Bin Xu, Shouguo Zhong, Jintian Wu *, Yujuan Zhou, Yongbin Yang, Qian Li and Tao Jiang

School of Minerals Processing and Bioengineering, Central South University, Changsha 410083, China; xubincsu@csu.edu.cn (B.X.); 205612106@csu.edu.cn (S.Z.); 185606015@csu.edu.cn (Y.Z.); ybyangcsu@126.com (Y.Y.); csuliqian@126.com (Q.L.); jiangtao@csu.edu.cn (T.J.)
* Correspondence: 195612116@csu.edu.cn

Abstract: A comprehensive recovery process for the selective separation and enrichment of copper, zinc and iron minerals from a polymetallic ore was developed, which consisted of copper flotation, zinc flotation, and iron magnetic separation, and the adsorption mechanism of the copper collector Z-200 (O-isopropyl-N-ethyl thionocarbamate) was also studied in this work. The contents of the main valuable metallic elements of Cu, Zn and Fe in the ore were respectively 0.61%, 1.68% and 14.17%, and they mainly existed as chalcopyrite, sphalerite and magnetite, whose dissemination relationship was complex. Under the optimal conditions of this process, the recoveries of Cu, Zn and Fe in their respective concentrates reached 86.1%, 87.6% and 77.8%, and their grades were separately 20.31%, 45.97% and 63.39%. This process realized the selective separation and beneficiation of copper, zinc, and iron minerals from the ore, and had promising industrial application prospects. The adsorption configuration analysis demonstrated that the steadiest adsorption configurations of Z-200 on the surfaces of chalcopyrite, sphalerite and magnetite were the simultaneous adsorption of carbonyl S together with the O atom. Compared with sphalerite and magnetite, Z-200 was more prone to adsorb on the chalcopyrite surface. The Mulliken charge population and bond length analyses manifested that Z-200 chemically adsorbed on the chalcopyrite surface by forming a normal covalent bond and a back donation covalent bond, and the normal covalent bond played a leading role. The chemisorption of Z-00 was supported by the FTIR spectrum analysis result.

Keywords: Z-200; copper-zinc-iron polymetallic ore; separation and enrichment; adsorption mechanism

1. Introduction

Iron, copper, and zinc are presently the first, third and fourth most widely consumed metals in the world, and they are indispensable raw materials in automobile, aviation, construction, mechanism, shipping, and other industries [1–3]. With the continuous development of the national economy, the consumption of copper, zinc, and iron mineral resources have increased rapidly [4,5]. But the available simple copper, zinc, and iron ore resources in China are very limited, which cannot meet the domestic demand [6–10]. Copper, zinc, and iron exist in China mainly in the form of complex polymetallic ore. Therefore, the comprehensive utilization of copper-zinc-iron polymetallic ore is very significant, which is also an effective way to support the sustainable development of China's copper, zinc, and iron industries.

The usual way for separating iron minerals from copper and zinc sulphide minerals is magnetic separation, and flotation is the most common method of enriching the copper and zinc [11–16]. Therefore, a combined flotation-magnetic separation process is often used to separate and enrich copper, zinc, and iron from a polymetallic ore. But it is still very difficult to achieve the complete separation of copper and zinc by flotation [17,18]. The main reasons are as follows: (a) copper and zinc minerals are embedded in each other tightly,

which makes it difficult to dissociate the copper and zinc minerals monomer; (b) during the grinding process, copper ions in the slurry are adsorbed on the surface of sphalerite, resulting in that sphalerite has similar floatability with chalcopyrite [19–22]; (c) the copper and zinc sulphide minerals are prone to be oxidized, which leads the deterioration of their floatability [23–25]. Formulating a reasonable beneficiation process and selecting an appropriate reagent regime based on ore characteristics are the keys to separate copper and zinc sulphide minerals. The main processes of flotation separation of copper and zinc sulphide minerals include differential flotation, mixed flotation, and iso-flotation [26]. The characteristic of mixed flotation, is that as much copper and zinc sulphide minerals as possible are floated out together after the first grinding stage. The mixed concentrate is reground for further separation of these metals by flotation. The disadvantage of this process is that the mixed concentrate contains many reagents, which makes the subsequent minerals separation difficult [27]. The feature of iso-flotation is that the copper sulphide minerals and part of the zinc sulphide minerals with good floatability are floated at the same time. Then the copper and zinc minerals in the mixed concentrate are separated after its regrinding, and the zinc minerals with poor floatability in the tailings are separately floated off. So, this kind of process is complicated [28]. Differential flotation allows the copper minerals to be floated first and then the zinc minerals are subsequently floated from the copper tailings, however, it requires high selectivity of the copper collector. In industry, the simplicity of this process combined with the high selectivity of the collector Z-200 (O-isopropyl-N-ethyl thionocarbamate) promotes it to be used widely [29].

The primary aim of this study was to develop a comprehensive recovery process for the selective separation and beneficiation of copper, zinc, and iron from a polymetallic ore. First, the process mineralogy of the polymetallic ore was studied to provide a theoretical basis for the design of a suitable separation process. Then, the differential flotation separation experiments for copper and zinc minerals, and the magnetic separation experiments for the iron minerals were performed to obtain the optimum process flow and corresponding conditions. Afterwards, the closed-circuit and reuse of return water experiments were carried out to investigate the effects of middling return and reuse of return water on recovery of valuable metals. Finally, the adsorption configurations of the copper collector Z-200 on the mineral crystal planes were constructed, and the adsorption mechanism of Z-200 for chalcopyrite was studied [30,31].

2. Experimental Work

2.1. Materials and Reagents

The chemical composition of the polymetallic ore is shown in Table 1, and the contents of Fe, Cu and Zn were 14.17%, 0.61% and 1.68%, respectively. The reagents used in this study were all analytically pure, and the water used was tap water.

Table 1. Chemical composition of the polymetallic ore (%).

Element	Fe	Cu	Zn	SiO_2	Al_2O_3	CaO	MgO
Content	14.17	0.61	1.68	18.16	4.75	19.48	9.04
Element	K_2O	Na_2O	TiO_2	P_2O_5	C	S	Others
Content	0.40	0.34	0.10	0.05	1.88	4.74	8.93

2.2. Experiment and Analysis Methods

2.2.1. Flotation Experiment

The raw ore needed to be finely ground before flotation to fully dissociate the mineral monomers. A Cu^{2+} deactivator ($C_9H_8Na_2O_4$, Na_2S, EDTA, or $(NH_4)_2S_2O_3$) was added to eliminate the activation of Cu^{2+} on sphalerite during grinding. A total of 1000 g ground ore and a proper amount of water were put into a single-trough flotation machine with the stirring speed of 1700 rpm, where the pulp concentration was 25%. Firstly, CaO as the pH regulator and $Na_2O \cdot nSiO_2$ as the dispersant were respectively added to the pulp, and then

the inhibitor, collector, and foaming agent of terpineol were added in sequence. During these steps, the pulp was stirred for 3 min after every addition of a reagent. Finally, the froth product (i.e., concentrate) and tailings were obtained after aerating for a few minutes, both of which were filtered, dried, weighed and analysed for elemental content.

2.2.2. Magnetic Separation Experiment

The primary iron mineral (i.e., magnetite) in this polymetallic ore could not be effective separated by flotation, and most of it entered the zinc flotation tailings. Magnetic separation of magnetite from the tailing was carried out in a CRIMM-φ400 $\times$ 300 circular drum magnetic separator (Changsha Institute of Mining and Metallurgy, Changsha, China). The obtained iron concentrate and the tailings were dried and then analysed for elemental content.

2.2.3. Simulating Calculation Method

The calculations were completed using the CASTEP module in the Material Studio 7.0 program (Accelrys, San Diego, CA, USA), in which the first-principles density functional theory was adopted [32–36]. According to the crystal lattice parameters of the mineral, the unit cell was constructed and optimized. For the optimization of the cleavage plane of the mineral, the appropriate atomic layers and vacuum layer thickness were selected. For the calculation of adsorption process, the distance between the active atom of the collector and the corresponding metal atom on the mineral surface was smaller than the sum of the radii of these two atoms. The geometric structural optimization of the adsorption configurations of Z-200 on the chalcopyrite (112), sphalerite (110), and magnetite (110) planes, and the Mulliken population analysis for the adsorption of Z-200 on the chalcopyrite (112) plane were calculated by using the same parameters. The PBE gradient correction function within the generalized gradient approximation (GGA) was used as the exchange correlation function, and the interaction between the valence electron and the ionic core was presented by Ultra-soft Pseudopotential. The convergence criteria for the structural optimization and energy calculation were: maximum displacement tolerance of 2.0×10^{-3} Å, maximum interatomic force tolerance of 0.05 eV/Å, maximum energy tolerance of 2.0×10^{-5} eV/atom, and maximum internal stress tolerance of 0.1 GPa.

2.2.4. FTIR Spectrum Analysis

First, 1 g of -38 μm chalcopyrite and 50 mL pure water were put into a beaker for ultrasonic cleaning, which lasted for 3 min. The supernatant was poured out, and then the collector together with an appropriate amount of water was added to the beaker. After magnetic stirring for 30 min, the obtained precipitate was washed three times, and then was dried under vacuum for 24 h at room temperature. The prepared sample as described above was mixed with a certain amount of KBr and further ground to -2 μm, and afterward the mixture was pressed into a thin sheet for test.

3. Results and Discussion

3.1. Process Mineralogy of the Polymetallic Ore

3.1.1. Mineralogical Composition

The XRD spectrogram (Figure 1) indicated that there were several kinds of minerals in the polymetallic ore, and its detailed mineral composition is shown in Table 2. These reveal that chalcopyrite, sphalerite, and magnetite were the main valuable minerals, and diopside, chlorite, calcite, gypsum and tremolite were the main gangue minerals. Besides, there was a small amount of quartz and limonite.
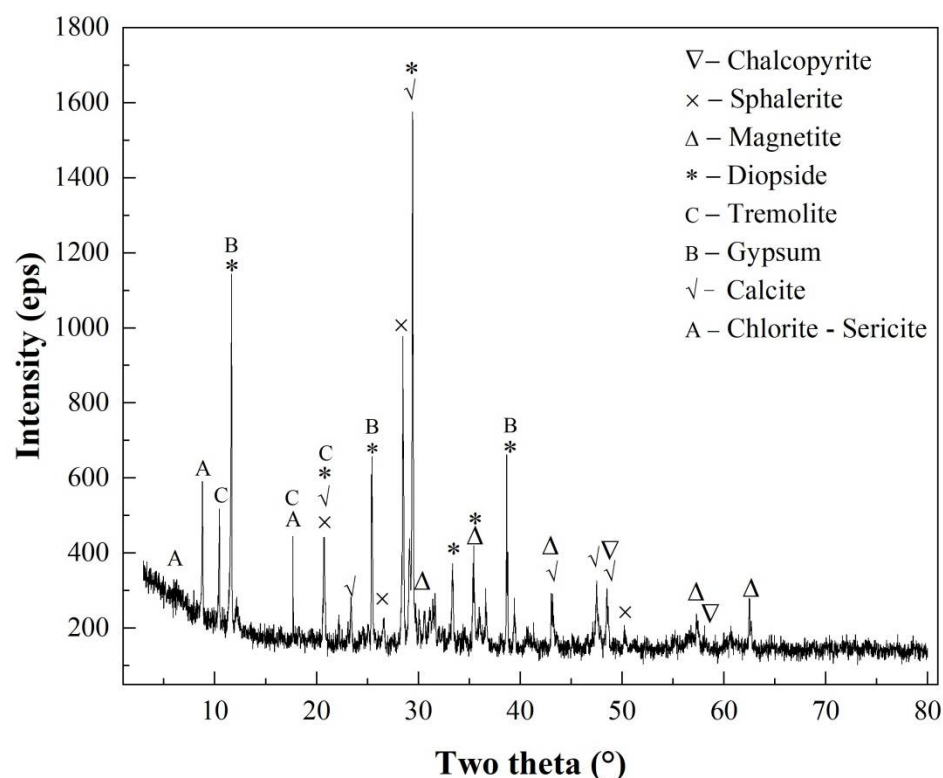
Figure 1. XRD spectrogram of the polymetallic ore.

Table 2. Mineral composition of the polymetallic ore (%).

Mineral	Chalcopyrite	Sphalerite	Magnetite	Diopside	Chlorite	Calcite
Content	1.38	2.41	13.40	19.24	16.56	15.60
Mineral	**Gypsum**	**Tremolite**	**Quartz**	**Limonite**	**Pyrite**	**Others**
Content	13.62	11.13	2.15	0.92	0.52	3.07

3.1.2. Phase Distribution of Main Elements

The back scattered electron (BSE) image and surface scan maps of main elements in the polymetallic ore are shown in Figure 2. The distribution areas of the elements sulphur, copper and zinc overlapped greatly, such as at site 2 and 3, which showed that the elements copper and zinc mainly existed in the form of sulphide. The distribution areas of the elements iron and oxygen overlapped more (such as at site 1), and that of the elements iron and silicon, aluminium, calcium, and magnesium overlapped in a small part (such as at site 4). This demonstrated that the element iron mainly existed in the form of oxide, and a small part of it occurred in the form of aluminosilicate. The results of the chemical phase analysis of copper, zinc, and iron are shown in Tables 3–5. As indicated, the primary phases of copper, zinc, and iron separately were chalcopyrite, sphalerite and magnetite, and their contents in these minerals were 0.48%, 1.61% and 9.63%, respectively.

Table 3. Copper chemical phase analysis of the polymetallic ore (%).

| Phase	Chalcopyrite	Bornite	Covellite	Cuprite	Total Copper
Cu Content	0.48	0.11	0.012	0.006	0.608
Distribution	78.95	18.09	1.97	0.99	100.00
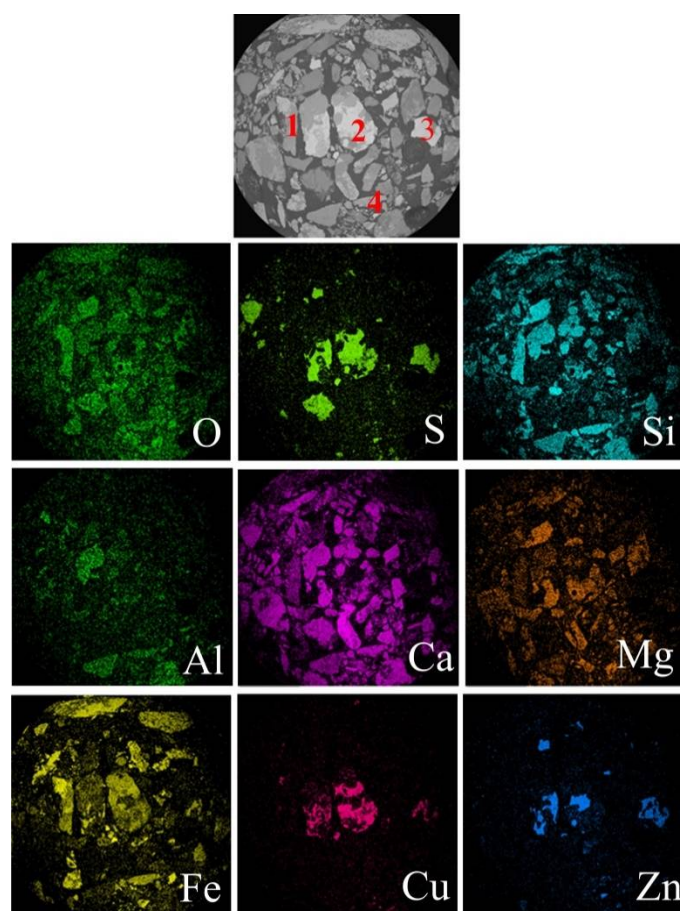
Figure 2. The SEM backscattered electron image and surface scan maps of main elements in the polymetallic ore (1—Iron oxide; 2,3—Copper-zinc sulphide; 4—Aluminosilicate).

Table 4. Zinc chemical phase analysis of the polymetallic ore (%).

Phase	Sphalerite	Silicate	Zinc Oxide	Total Zinc
Zn Content	1.61	0.05	0.02	1.68
Distribution	95.83	2.98	1.19	100.00

Table 5. Iron chemical phase analysis of the polymetallic ore (%).

Phase	Magnetite	Silicate	Hematite + Limonite	Chalcopyrite
Fe Content	9.63	3.01	0.66	0.42
Distribution	67.96	21.24	4.66	2.97
Phase	**Pyrite**	**Carbonate**	**Pyrrhotite**	**Total iron**
Fe Content	0.24	0.18	0.03	14.17
Distribution	1.69	1.27	0.21	100.00

3.1.3. Dissemination Characteristics

The dissemination characteristics of chalcopyrite, sphalerite and magnetite were as follows: (1) chalcopyrite in emulsion droplets with the size of 2–3 µm was distributed in sphalerite (Figure 3a), and chalcopyrite strips with a thickness of 2–4 µm could be seen around sphalerite particles (Figure 3b); (2) fine grained chalcopyrite whose diameter was generally 1–20 µm was dispersed in coarse magnetite particles (Figure 3c), and sometime chalcopyrite and magnetite contacted one another in linear and harbour forms (Figure 3d); (3) sphalerite was in linear and harbour contact with magnetite (Figure 3b).

Figure 3. Association and dissemination properties of the main minerals. (Cha-chalcopyrite, Sph-sphalerite, Mt-magnetite, Q-quartz. (**a**) Chalcopyrite was distributed in sphalerite; (**b**) Chalcopyrite contacted with magnetite and sphalerite; (**c**) Chalcopyrite was distributed in magnetite; (**d**) Chalcopyrite contacted with magnetite).

3.1.4. Monomer Dissociation of the Main Valuable Minerals

The monomer dissociations of chalcopyrite, sphalerite, and magnetite in different particle sizes of the polymetallic ore are separately shown in Tables 6–8. The finer the size of ore, the higher the dissociation degree of the mineral monomer. In the +200-mesh size fraction, the dissociation degrees of chalcopyrite, sphalerite, and magnetite monomers were only 27.12%, 60.37% and 24.40%, respectively. However, in the −325~+400-mesh size fraction, the dissociation degrees of chalcopyrite, sphalerite and magnetite monomers were 81.69%, 83.16% and 90.93%, respectively. Therefore, the fine grinding of polymetallic ore was essential to the subsequent flotation separation.

Table 6. Monomer dissociation of chalcopyrite in each size fraction.

Grade (Mesh)	Productivity (%)	Cu (%)	Chalcopyrite Monomer (%)	Conjuncture (%)						
				Sphalerite	Magnetite	Quartz	Pyroxene-Hornblende	Chlorite-Sericite	Calcite	Others
+200	11.5	0.41	27.12	14.07	6.97	12.55	22.43	12.17	2.92	1.77
−200~+250	5.0	0.54	61.67	12.65	1.16	11.28	6.73	4.75	1.16	0.58
−250~+325	17.5	0.57	78.22	6.74	0.59	4.48	4.54	3.76	1.10	0.57
−325~+400	7.6	0.66	81.69	6.50	0.58	4.40	2.11	3.70	0.82	0.20
−400	58.4	0.65	89.22	3.85	0.48	4.35	0.96	0.56	0.48	0.10
Total	100	0.61								

Table 7. Monomer dissociation of sphalerite in each size fraction.

Grade (Mesh)	Productivity (%)	Zn (%)	Sphalerite Monomer (%)	Conjuncture (%)						
				Chalcopyrite	Magnetite	Quartz	Pyroxene-Hornblende	Chlorite-Sericite	Calcite	Others
+200	11.5	1.33	60.37	15.55	4.07	3.34	8.70	5.18	1.90	0.89
−200~+250	5.0	1.78	65.00	13.93	3.25	3.74	7.49	4.24	1.75	0.60
−250~+325	17.5	1.76	76.85	6.12	1.24	2.93	7.02	3.93	1.58	0.33
−325~+400	7.6	1.88	83.16	5.51	0.15	2.68	3.13	0.45	0.44	0.30
−400	58.4	1.69	93.94	1.14	0.10	2.57	1.50	0.30	0.20	0.25
Total	100	1.68								

Table 8. Monomer dissociation of magnetite in each size fraction.

Grade (Mesh)	Productivity (%)	Fe (%)	Magnetite Monomer (%)	Conjuncture (%)						
				Chalcopyrite	Sphalerite	Quartz	Pyroxene-Hornblende	Chlorite-Sericite	Calcite	Others
+200	11.5	11.45	24.40	8.66	1.60	37.43	18.93	5.13	3.21	0.64
−200~+250	5.0	14.98	61.39	6.11	0.17	16.17	7.59	6.27	1.97	0.33
−250~+325	17.5	16.47	83.23	1.63	0.10	7.75	2.71	2.80	1.50	0.28
−325~+400	7.6	19.24	90.93	1.31	0.08	2.96	1.97	2.23	0.26	0.26
−400	58.4	13.30	94.42	0.05	0.03	2.67	1.14	1.29	0.20	0.20
Total	100	14.17								

3.2. Beneficiation Experiments

3.2.1. Reagent Regime of Copper and Zinc Flotations

The separation and enrichment of copper and zinc minerals from the raw ore by flotation mainly depend on the reagent regime and the flotation process. The Z-200 (O-isopropyl-N-ethyl thionocarbamate) collector selected in this experiment is a common and efficient copper collector. To effectively inhibit zinc flotation during the copper flotation process, $ZnSO_4$ and Na_2SO_3 were selected as combined inhibitors. The effects of the collector and inhibitor dosages on copper flotation were first studied, and the experimental flow charts and results are shown in Figures 4 and 5, respectively. Under the dosage for $ZnSO_4 + Na_2SO_3$ of 1500 + 500 g/t, the grade of copper concentrate decreased, and copper recovery increased with the increase of the Z-200 dosage. When the dosage reached 30 g/t, its further increase would cause a substantial drop in the copper grade, but not make a significant improvement in copper recovery. The zinc recovery of concentrate usually decreased with increasing zinc inhibitor dosage. So, the copper grade and recovery both increased with the increase of $ZnSO_4 + Na_2SO_3$ dosage in the range of 1200 + 400 g/t to 1800 + 600 g/t, as shown in Figure 5b. After that, there was no obvious change in the copper grade, and the recovery dropped. Therefore, the optimal dosages of Z-200 and $ZnSO_4 + Na_2SO_3$ in the rough copper flotation were 30 g/t and 1800 + 600 g/t, respectively.
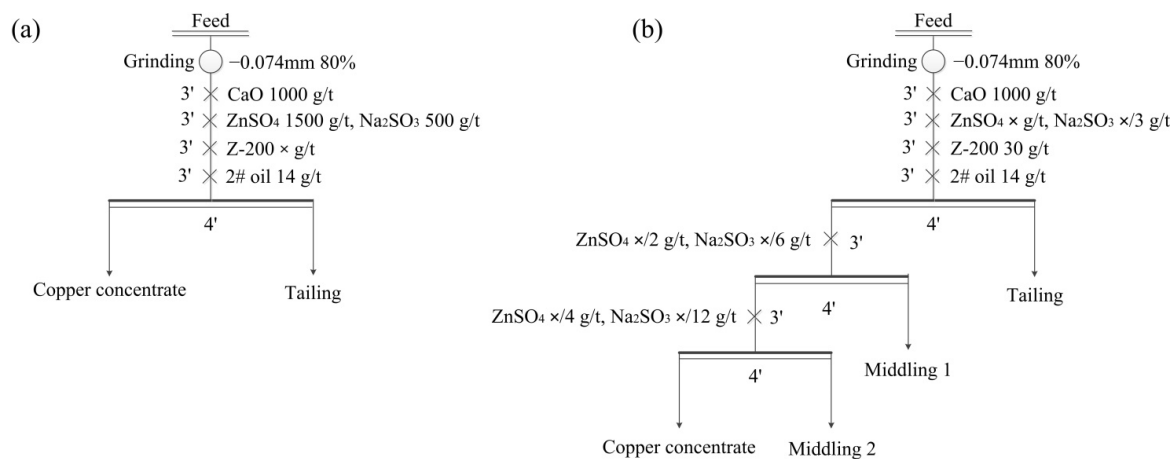
Figure 4. Experimental flow charts for the effects of Z-200 (**a**) and $ZnSO_4 + Na_2SO_3$ (**b**) dosages on copper flotation.
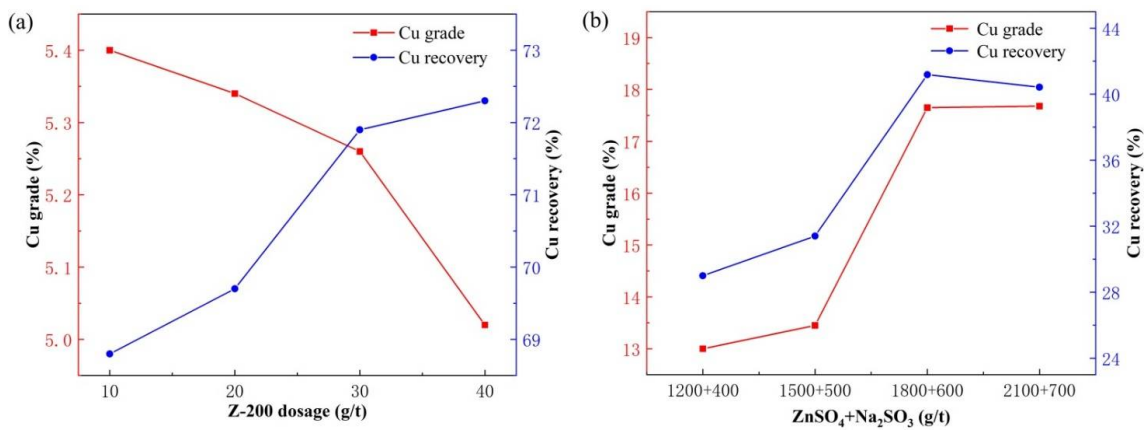
Figure 5. Effects of Z-200 (**a**) and ZnSO$_4$ + Na$_2$SO$_3$ (**b**) dosages on copper flotation.

Next, the effects of the dosages for the collector butyl xanthate (BX) and the activator CuSO$_4$ on zinc flotation were investigated based on the flow charts in Figure 6, where the feed was copper flotation tailings, and the results are shown in Figure 7. It can be concluded from Figure 7a that the recovery and grade of zinc concentrate both increased with the increase of BX dosage in the range of 60–80 g/t, and when beyond this range they were reduced. Thus, the optimal BX dosage was 80 g/t in rough zinc flotation. From Figure 7b, when CuSO$_4$ dosage was less than 500 g/t, the zinc grade and recovery both increased with increase in the dosage. After 500 g/t, the recovery did not increase significantly, and the grade declined. So, the optimal dosage of CuSO$_4$ in rough zinc flotation was 500 g/t.
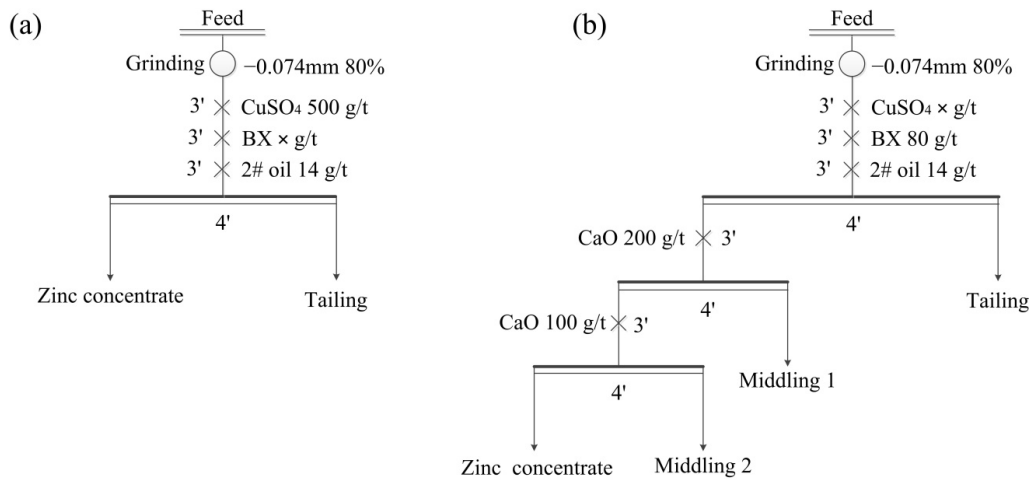
Figure 6. Experimental flow charts for the effects of BX (**a**) and CuSO$_4$ (**b**) dosages on zinc flotation.
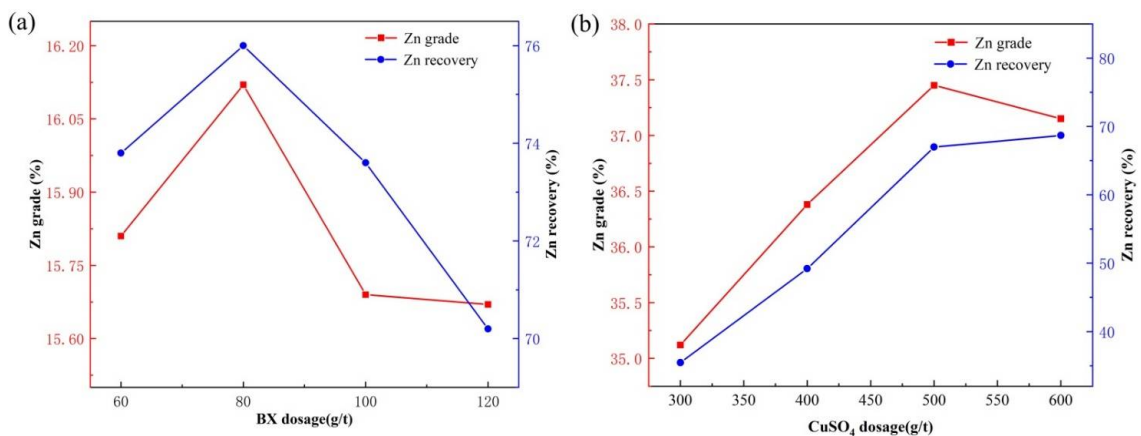
Figure 7. Effects of BX (**a**) and CuSO$_4$ (**b**) dosages on zinc flotation.

In the grinding process, sphalerite would been activated by Cu^{2+} deriving from chalcopyrite, which made its floatability close to that of chalcopyrite [37], so it was difficult to separate copper and zinc minerals by flotation. By adding a Cu^{2+} deactivator in the ball mill, the Cu^{2+} activation effect could be effectively relived. Without adding CaO and Na_2O $nSiO_2$, the effects of the deactivator type and dosage on the rough copper flotation were studied according to the flow chart in Figure 8, and the results are shown in Figure 9. At dosages of 300 g/t, compared with NaS_2, EDTA and $(NH_4)_2S_2O_3$, when $C_9H_8Na_2O_4$ was the Cu^{2+} deactivator, the Cu recovery and grade of copper concentrate, and Zn recovery and grade of tailings, all reached the maximum. Therefore, $C_9H_8Na_2O_4$ had the best deactivation performance. As indicated in Figure 9c,d, the above four indicators increased in 200 g/t−300 g/t and decreased in 300 g/t−500 g/t with the increase of the $C_9H_8Na_2O_4$ dosage, which illustrated that the copper and zinc minerals were separated the most thoroughly at 300 g/t. As a result, the $C_9H_8Na_2O_4$ dosage in rough copper flotation was chosen to be 300 g/t.
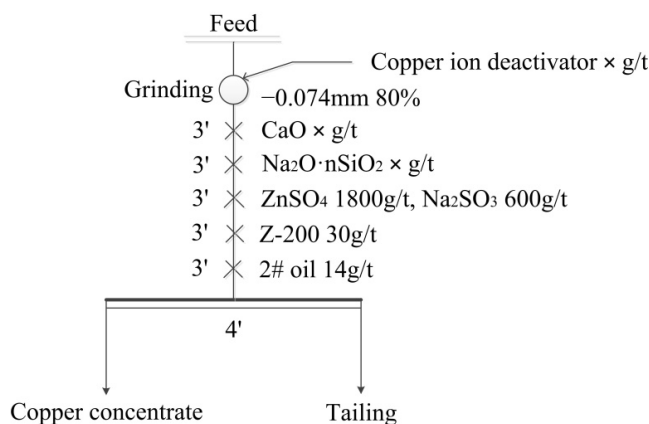
Figure 8. Experimental flow chart of the effects of copper ion deactivator, CaO and Na_2OnSiO_2 on rough copper flotation.
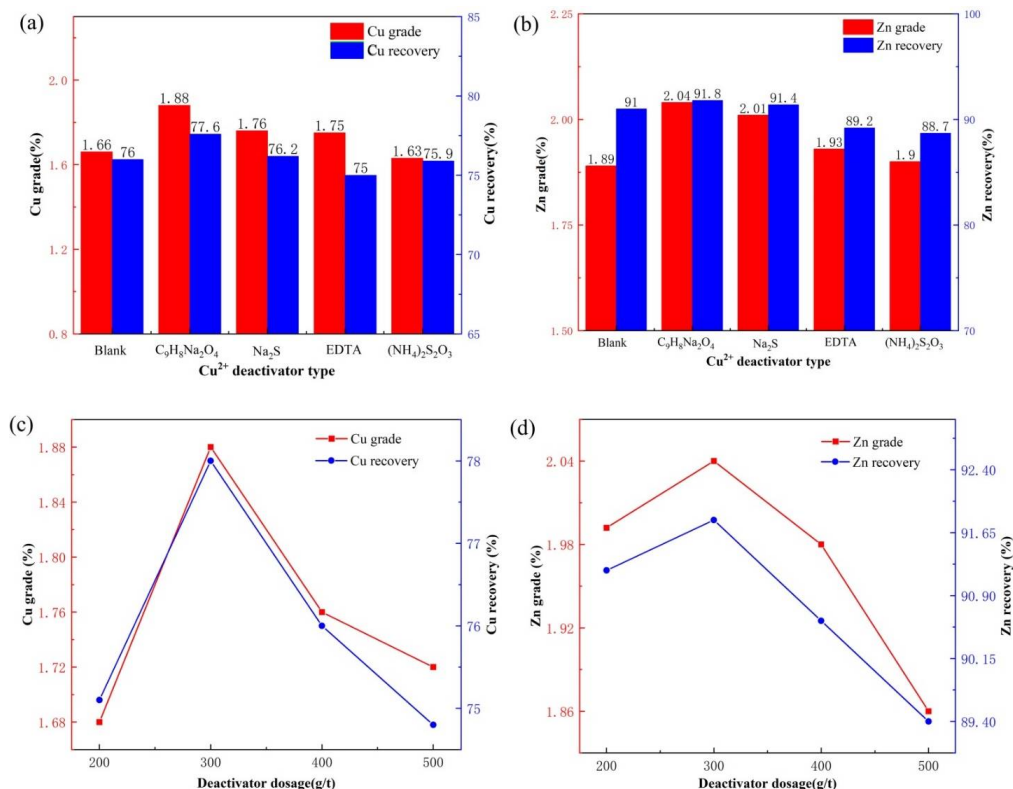
Figure 9. Effects of deactivator type (**a**,**b**) and dosage (**c**,**d**) on rough copper flotation.

Under weak alkaline conditions, Z-200 had a better collecting performance for chalcopyrite [38], so CaO was usually added into the pulp. Without adding the Cu^{2+} deactivator and $Na_2O \cdot nSiO_2$, the influence of the CaO dosage on rough copper flotation was studied. The experimental flow chart is shown in Figure 8, and the results are given in Figure 10a,b. The Cu recovery and grade of concentrate and Zn recovery of tailings all first increased and then decreased with the increase of CaO dosage, they reached the maximum when CaO was 2000 g/t, and the Zn grade of tailings was less influenced by CaO. Thus, the optimum dosage of CaO in rough copper flotation was 2000 g/t.
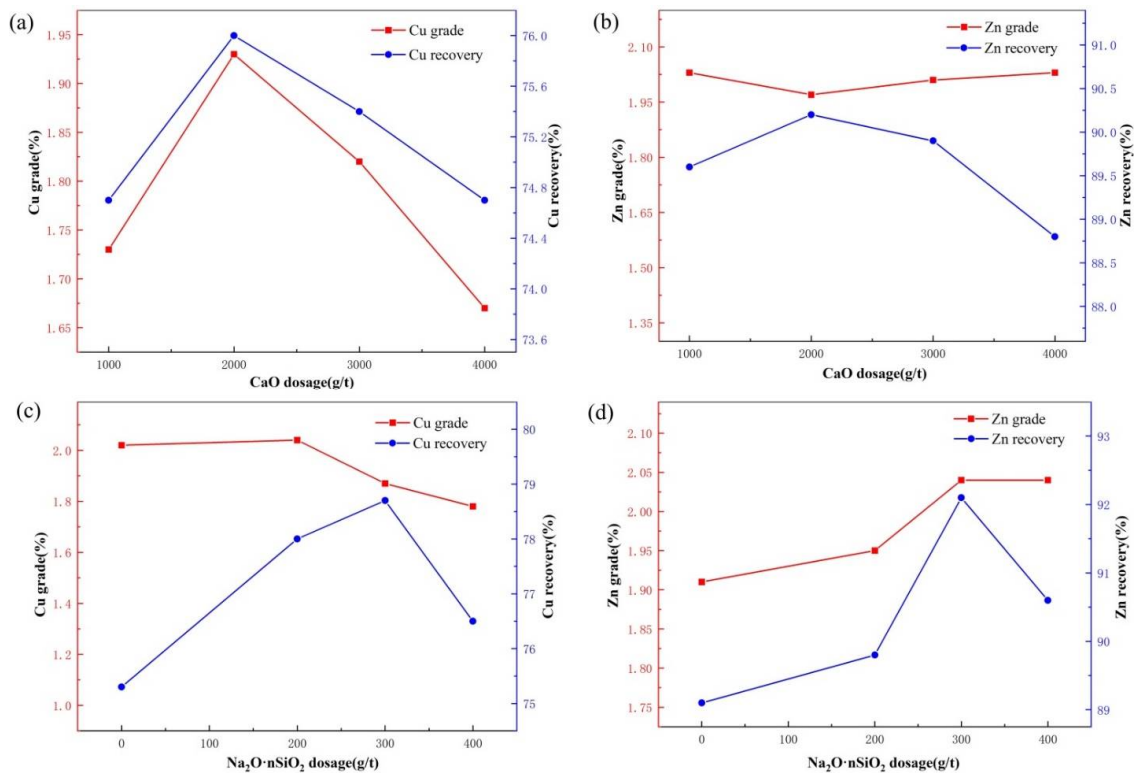
Figure 10. Effects of CaO (**a**,**b**) and $Na_2O \cdot nSiO_2$ (**c**,**d**) dosages on rough copper flotation.

The addition of the dispersant $Na_2O \cdot nSiO_2$ would effectively avoid the serious sliming mainly caused by overground mineral grains such as chlorite and calcite, and thus improved the flotation separation effectiveness. When the $C_9H_8Na_2O_4$ concentration was 300 g/t and CaO was 2000 g/t, the experimental flow chart of the effect of dispersant dosage is shown in Figure 8 and the results are given in Figure 10c,d. The Cu recovery of concentrate and Zn recovery of tailings both increased with the increase of $Na_2O \cdot nSiO_2$ dosage in the range of 0 g/t−300 g/t. After 300 g/t, these two recoveries dropped with the further dosage increase. So, the optimal dosage of $Na_2O \cdot nSiO_2$ for rough copper flotation was 300 g/t.

3.2.2. Numbers of Cleaning Cycles for Copper and Zinc Flotations

Increasing the numbers of cleaning cycles could improve the grade of concentrate. The experimental flow charts for the effect of numbers of cleaning cycles for copper and zinc flotations are shown in Figures 11 and 12, and the results are shown in Figure 13. The grades of copper and zinc concentrates both increased sharply with the increase in number of cleaning cycles in the range of 1–3, while after three cycles the increase was insignificant. Therefore, the optimal number of copper and zinc cleaning cycles both were 3.
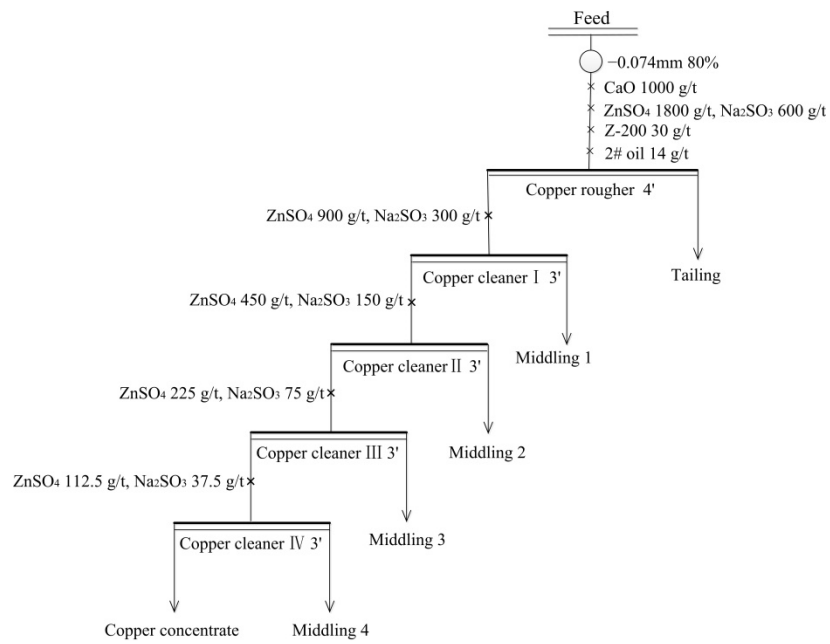
Figure 11. The experimental flow charts of the effect of the number of cleaning cycles in copper flotation.
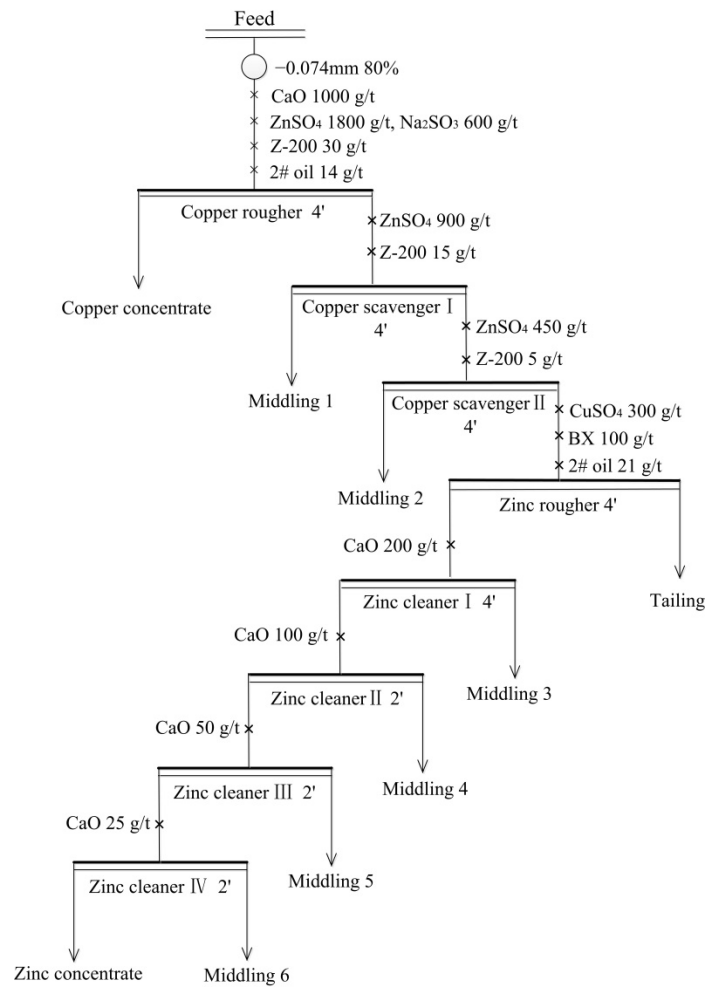

**Figure 12.** The experimental flow chart of the number of cleaning cycles in zinc flotation.
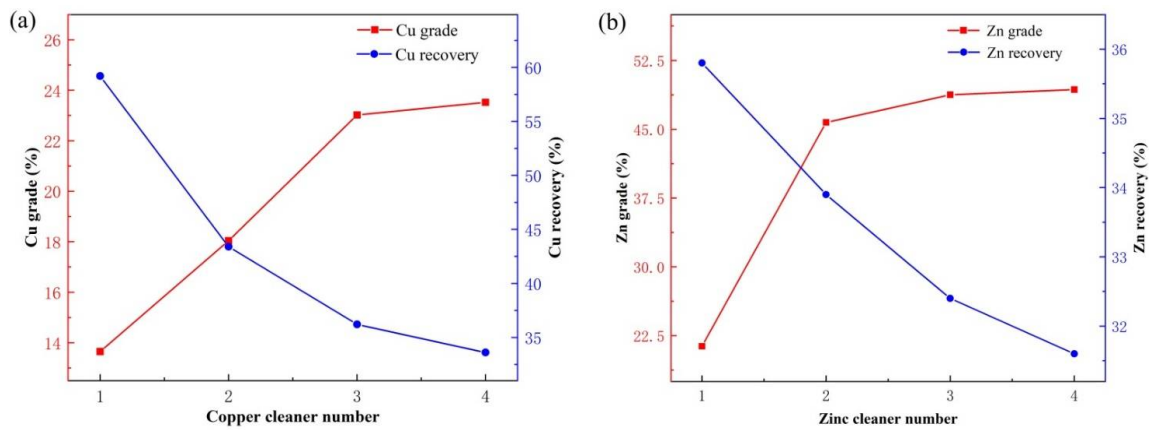
Figure 13. Effects of the number of cleaning cycles on copper (**a**) and zinc (**b**) flotations.

3.2.3. Magnetic Field Intensity of Iron Magnetic Separation

Iron in zinc tailings, mainly existed as magnetite having strong magnetism, so iron could be effectively recovered by magnetic separation. The experimental flow chart of the effect of magnetic intensity is shown in Figure 14, and the results are given in Figure 15. Iron recovery of magnetic concentrate increased greatly, and iron grade decreased moderately, with the increase of magnetic intensity in 100–140 mT. With the further increase of magnetic intensity, iron recovery had no significant change. Therefore, the optimal magnetic intensity of magnetic separation was 140 mT.
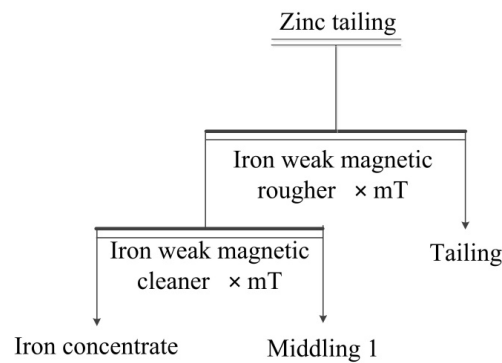
Figure 14. Experimental flow chart of the effect of magnetic intensity.
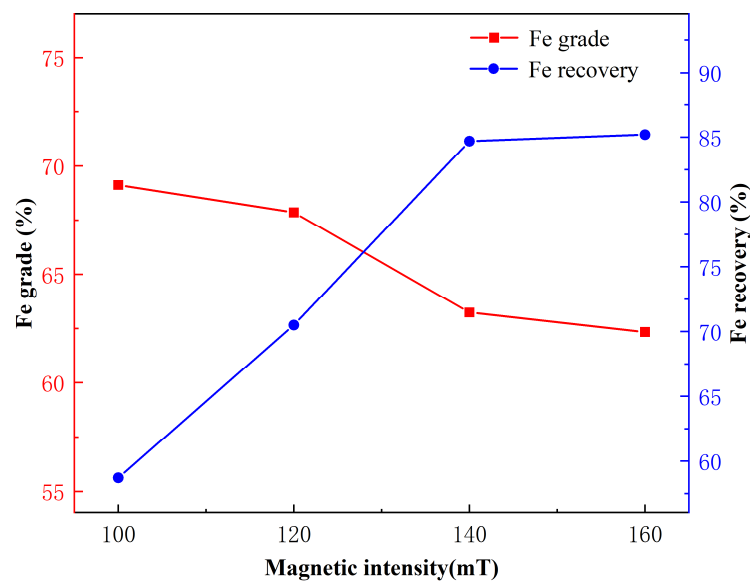
Figure 15. The effect of magnetic intensity on iron magnetic separation.

3.2.4. Closed-Circuit Experiment

A comprehensive recovery process was developed in this work to realize the separation and enrichment of copper, zinc, and iron minerals from a polymetallic ore, where the scavenger numbers of copper and zinc flotations and iron magnetic separation, respectively, were 2, 2 and 1, based on industry experience. To evaluate the effectiveness of this process, a closed-circuit experiment whose flowchart is shown in Figure 16 was carried out, in which the reagent dosages were decreasing in order from rough flotation to each cleaner stage and scavenger flotations. The cyclic number of this closed-circuit test was 5, and the average values of the last three cyclic tests results are listed in the Table 9. The grades of copper, zinc, and iron in their respective concentrates arrived at 20.31%, 45.97% and 63.39%, and their recoveries reached 86.1%, 87.6% and 77.8%, respectively. So, the separation and enrichment of copper, zinc and iron minerals were well realized by the developed comprehensive recovery process. In addition, silver also was enriched in the copper concentrate, whose Ag grade and recovery separately was 532 g/t and 79.5%.

Table 9. The results of the closed-circuit experiment of the developed comprehensive recovery process.

| Product	Yield/%	Grade/%				Recovery/%			
		Copper	Zinc	Iron	Silver *	Copper	Zinc	Iron	Silver
Copper concentrate	2.6	20.31	4.78	10.18	532	86.1	7.4	1.9	79.5
Zinc concentrate	3.2	1.59	45.97	10.21	42	8.3	87.6	2.3	7.7
Iron concentrate	17.4	0.02	0.09	63.39	4	0.6	0.9	77.8	4.0
Tailing	76.8	0.04	0.09	3.32	2	5.0	4.1	18.0	8.8
Raw ore	100.0	0.61	1.68	14.17	17.4	100	100	100	100

* Unit g/t.
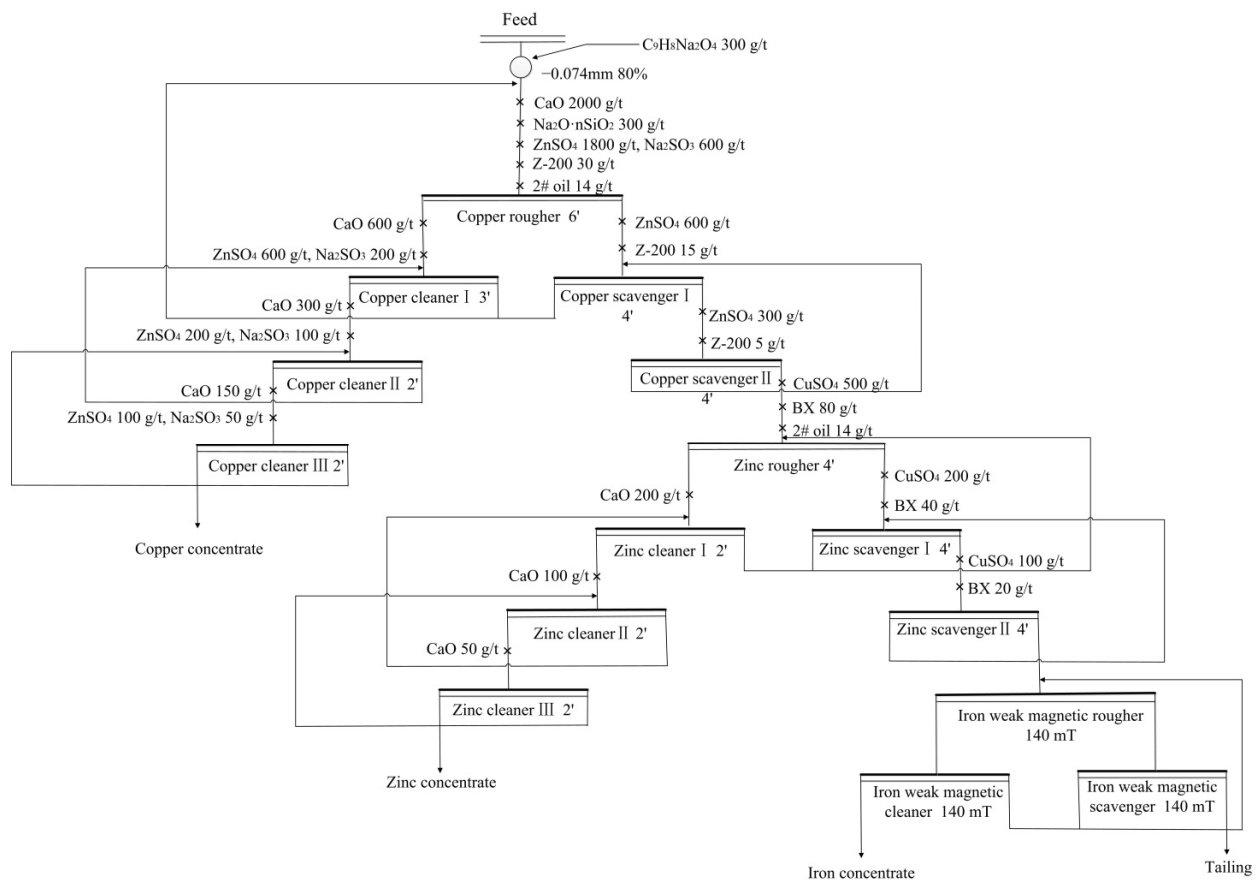
Figure 16. The flowchart of the closed-circuit experiment of the developed comprehensive recovery process.

3.2.5. Reuse of Return Water

The reuse of return water in the beneficiation process could save water resources and avoid environmental pollution caused by the discharge of beneficiation wastewater. Thus, a test for the reuse of return water was conducted to investigate its effect on copper and zinc flotations. The return water used here was the filtrate of the final tailings slurry from the closed-circuit experiment described in Section 3.2.4, and the use proportions of the return water mixed with fresh water before ball-milling were 0%, 20%, 40%, 60% and 80%. The experimental flowchart for the effect of return water reuse is shown in Figure 17, and the results are given in Figure 18. As indicated, the grades of copper and zinc in the respective concentrates and their recoveries did not change materially with the increase of the return water ratio. Therefore, the reuse of return water hardly had any adverse effect on the copper and zinc flotations.
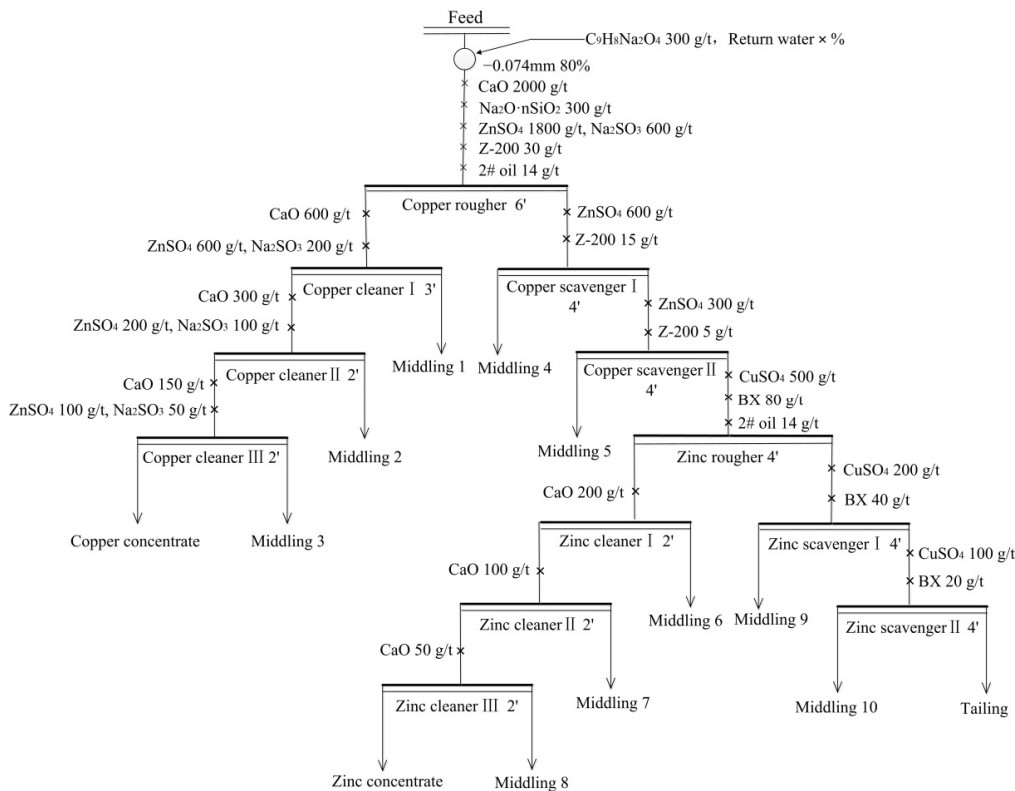

**Figure 17.** The experimental flowchart of reuse of return water.
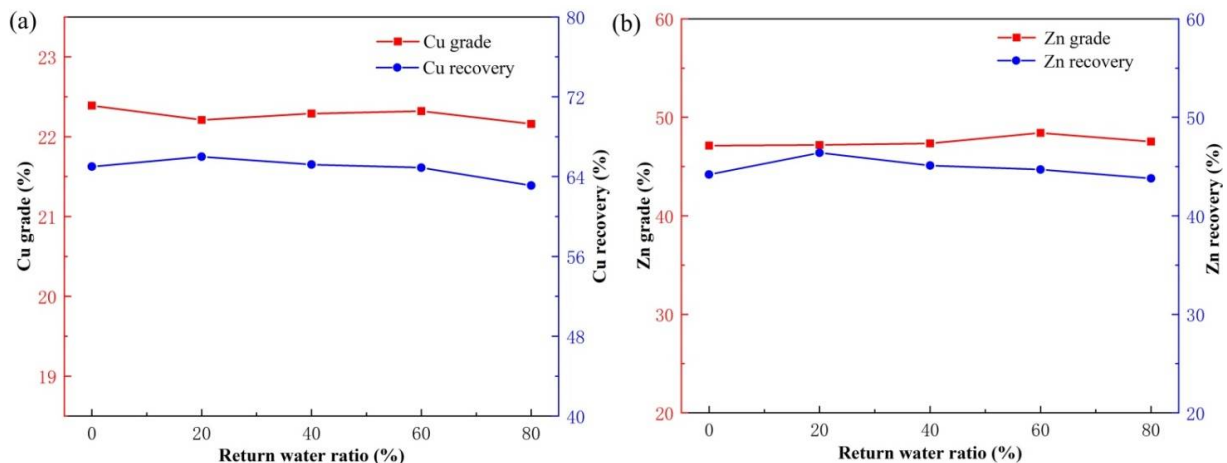
Figure 18. Effect of return water ratio on copper flotation (**a**) and zinc flotation (**b**).

3.3. Mechanism of Z-200 Adsorption

3.3.1. Adsorption Configuration Analysis

The preferential cleavage planes of chalcopyrite, sphalerite and magnetite were (112), (110) and (110) planes, respectively. The adsorption configurations of Z-200 on these crystal planes were studied by simulating calculation using Material Studio software, and the corresponding adsorption energies are given in Table 10. For all three crystal planes, the adsorption energy for the configuration of the simultaneous adsorption of carbonyl S together with the O atom was the lowest among the six configurations of Z-200, which meant that this configuration was the most stable for all these planes. The adsorption energies of the most stable configuration of Z-200 on the chalcopyrite (112) and sphalerite (110) planes were both negative, but that on the magnetite (110) plane was positive, manifesting that Z-200 could adsorb spontaneously on the chalcopyrite (112) and sphalerite (110) planes but not on the magnetite (110) plane. The adsorption energy of the chalcopyrite (112) plane was lower than that of the sphalerite (110) plane, suggesting that Z-200 was more prone to adsorb on the chalcopyrite (112) plane.

Table 10. Adsorption energies of adsorption configurations of Z-200 on different mineral crystal planes.

Adsorption Configuration	Adsorption Energy (kJ/mol)		
	Chalcopyrite (112) Plane	Sphalerite (110) Plane	Magnetite (110) Plane
Adsorption of carbonyl S	−19.45	−16.11	6.27
Adsorption of N	−9.79	−7.13	12.69
Adsorption of O	−15.90	−13.67	9.38
Simultaneous adsorption of carbonyl S together with N	−10.39	−9.94	10.38
Simultaneous adsorption of carbonyl S together with O	−21.89	−18.21	2.67
Simultaneous adsorption of N and O	−5.47	−4.22	14.39

3.3.2. Bond Length and Mulliken Charge Population Analyses

The six adsorption configurations of Z-200 on the chalcopyrite (112) plane are shown in Figure 19, where the bond length was marked. According to valence bond theory, the shorter the bond length, the stronger the electron localization, i.e., the more stable the bond. The adsorption bond of simultaneous adsorption of carbonyl S together with the O atom was the shortest, which further proved that this configuration was the most stable. Compared with the O adsorption bond, the length of the carbonyl S adsorption bond in this configuration was shorter, indicating that the interaction between the carbonyl S and the bonding Cu atom in chalcopyrite surface was stronger.

(a)

(b)
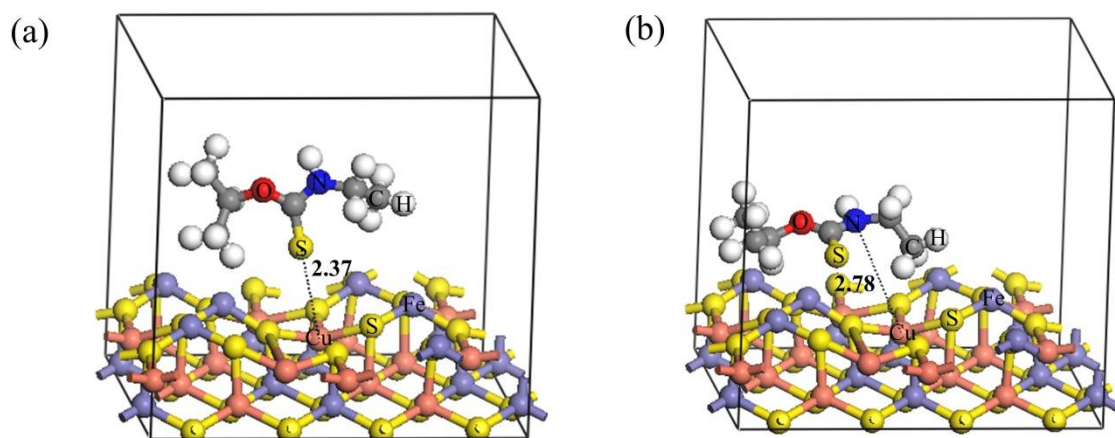
Figure 19. *Cont.*
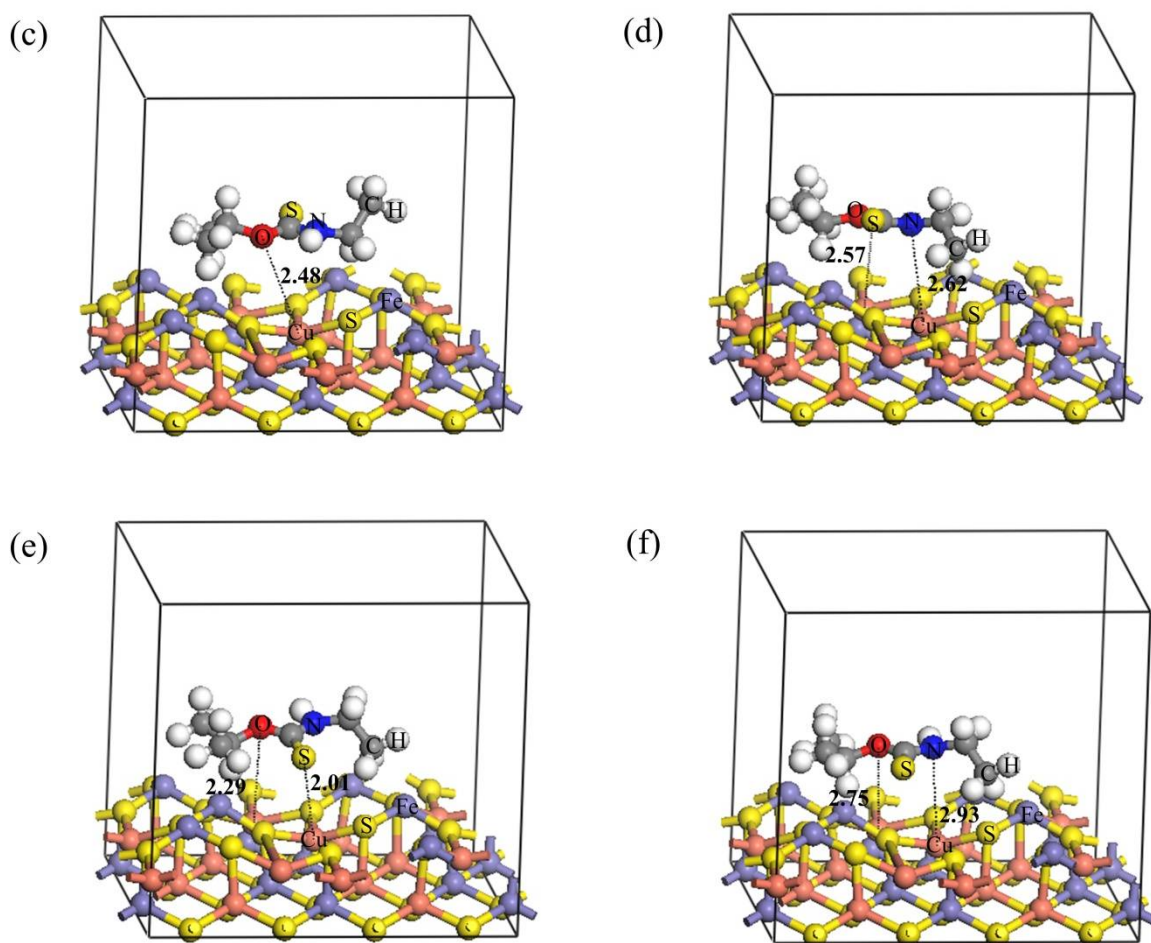
Figure 19. Optimized adsorption configurations of Z-200 on chalcopyrite (112) crystal plane ((**a**) adsorption of carbonyl S; (**b**) adsorption of N; (**c**) adsorption of O; (**d**) simultaneous adsorption of carbonyl S together with N; (**e**) simultaneous adsorption of carbonyl S together with O; (**f**) simultaneous adsorption of N and O).

The Mulliken charge populations of the bonding atoms before and after Z-200 adsorption on chalcopyrite (112) plane are displayed in Table 11. It could be speculated that the 3p orbital of carbonyl S of Z-200 offered electrons to 3d orbital of Cu atom in chalcopyrite surface to form a normal covalent bond during the chemisorption, while the 2p orbital of O atom in Z-200 accepted the electrons from the 3d orbital of Cu atom to form a back donation covalent bond.

Table 11. Mulliken charge populations of bonding atoms before and after adsorption.

Bonding Atom	Adsorption State	Electron Charge (e)			Charge Population
		s	p	d	
Carbonyl S	Before adsorption	1.82	4.41	0.00	−0.23
	After adsorption	1.82	4.35	0.00	−0.17
Cu$_{(S-Cu)}$	Before adsorption	0.61	0.43	9.74	0.23
	After adsorption	0.61	0.43	9.78	0.19
O Atom	Before adsorption	1.77	4.66	0.00	−0.44
	After adsorption	1.77	4.69	0.00	−0.47
Cu$_{(O-Cu)}$	Before adsorption	0.61	0.43	9.74	0.23
	After adsorption	0.60	0.42	9.67	0.32

3.3.3. FTIR Spectrum Analysis

The infrared spectra of Z-200, chalcopyrite, and Z-200-adsorbed chalcopyrite are presented in Figure 20. After the adsorption of Z-200, the infrared spectrum of chalcopyrite changed evidently, suggesting that Z-200 chemisorbed on the chalcopyrite surface [39–43]. Two new strong absorption peaks appeared at 1022.27 cm^{-1} and 1097.50 cm^{-1}, which could be separately attributed to C=S-S and C-O-S coupled vibrations. The possible reason for the formation of these two new peaks was that the O and S atoms of C-O and C=S bands in Z-200 separately obtained and lost some electrons when they reacted with Cu^{2+} on the chalcopyrite surface.
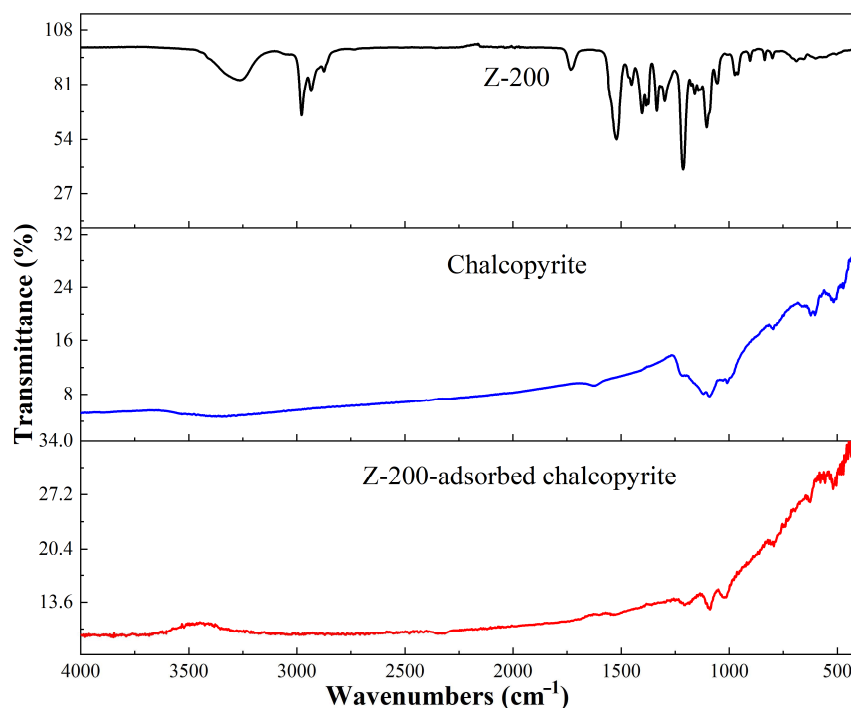
Figure 20. The FTIR spectra of Z-200, chalcopyrite, and Z-200-adsorbed chalcopyrite.

4. Conclusions

A comprehensive recovery process was developed to selectively separate and enrich copper, zinc and iron minerals from a polymetallic ore, and the adsorption mechanism of the copper collector Z-200 was also studied in this work. The following conclusions were obtained.

(1) The chemical composition and phase distribution analyses showed that the main valuable metallic elements in the polymetallic ore were Cu, Zn and Fe, and they mainly existed in the form of chalcopyrite, sphalerite, and magnetite, respectively. The dissemination characteristics analysis manifested that chalcopyrite, sphalerite and magnetite minerals were mainly in linear and harbour contact relationships, and furthermore enwrapped in each other. The monomer dissociation analysis indicated that the fine grinding of ore was essential to obtain a satisfactory result for the separation and enrichment of copper, zinc and iron minerals.

(2) A comprehensive process consisting of copper flotation, zinc flotation and iron magnetic separation was developed through systematic beneficiation experiments. Copper and zinc flotations were both composed of one rough, three cleaners and two scavengers, and their collectors were separately Z-200 and butyl xanthate, and iron magnetic separation included one rough, one cleaner and one scavenger. Under the optimal conditions, the recoveries of copper, zinc and iron in their respective concentrates reached 86.1%, 87.6% and 77.8%, and their grades separately reached 20.31%, 45.97% and 63.39%. It was demonstrated

through experiments that the reuse of return water of the beneficiation process had no evident adverse effect on the copper and zinc flotations.

(3) The adsorption configuration analysis showed that the steadiest adsorption configuration of Z-200 on all of the surfaces of chalcopyrite, sphalerite and magnetite was the simultaneous adsorption of carbonyl S together with the O atom, and Z-200 was most prone to adsorb on chalcopyrite surface. The Mulliken charge population and bond length analyses manifested that when Z-200 adsorbed on chalcopyrite surface the 3p orbital of carbonyl S of Z-200 offered electrons to the 3d orbital of the Cu atom on the surface to form a normal covalent bond, while the 2p orbital of the O atom in Z-200 accepted the electrons from the 3d orbital of the Cu atom to form a back donation covalent bond, and the stronger normal covalent bond plays a dominant role during the adsorption. The FTIR spectrum analysis also supported that Z-200 chemically adsorbed on the chalcopyrite surface.

References

1. Dong, Z.L.; Jiang, T.; Xu, B.; Yang, Y.B.; Li, Q. An eco-friendly and efficient process of low potential thiosulfate leaching-resin adsorption recovery for extracting gold from a roasted gold concentrate. *Cleaner Prod.* **2019**, *229*, 387–398. [CrossRef]
2. Dong, Z.L.; Jiang, T.; Xu, B.; Yang, J.K.; Chen, Y.Z.; Yang, Y.B.; Li, Q. Comprehensive recoveries of selenium, copper, gold, silver and lead from a copper anode slime with a clean and economical hydrometallurgical process. *Chem. Eng.* **2020**, *393*, 124762. [CrossRef]
3. Liu, G.; Jiang, K.; Zhang, B.; Dong, Z.; Zhang, F.; Wang, F.; Jiang, T.; Xu, B. Selective Flotation of Elemental Sulfur from Pressure Acid Leaching Residue of Zinc Sulfide. *Minerals* **2021**, *11*, 89. [CrossRef]
4. Wei, D.Z. *Solid Materials Separation*; Metallurgical Industry Press: Beijing, China, 2009.
5. Zhang, X.L.; Qin, Y.H.; Han, Y.X.; Li, Y.J.; Gao, P.; Li, G.F.; Wang, S.X. A potential ceramic ball grinding medium for optimizing flotation separation of chalcopyrite and pyrite. *Powder Technol.* **2021**, *392*, 167–178. [CrossRef]
6. Li, L.; Pan, D.; Li, B.; Wu, Y.; Wang, H.; Gu, Y.; Zuo, T. Patterns and challenges in the copper industry in China. *Resour. Conserv. Recycl.* **2017**, *127*, 1–7. [CrossRef]
7. Kuchar, D.; Fukuta, T.; Onyango, M.S.; Matsuda, H. Sulfidation treatment of copper-containing plating sludge towards copper resource recovery. *J. Hazard. Mater.* **2006**, *138*, 86–94. [CrossRef]
8. Spuerk, S.; Drobe, M.; Lottermoser, B.G. Evaluating resource efficiency at major copper mines. *Miner. Eng.* **2017**, *107*, 27–33. [CrossRef]
9. Singer, D.A. Future copper resources. *Ore Geol. Rev.* **2017**, *86*, 271–279. [CrossRef]
10. Zhang, L.; Chen, T.; Yang, J.; Cai, Z.; Sheng, H.; Yuan, Z.; Wu, H. Characterizing copper flows in international trade of China, 1975–2015. *Sci. Total Environ.* **2017**, *601–602*, 1238–1246. [CrossRef]
11. Hu, H.; Li, M.; Li, L.; Tao, X. Improving bubble-particle attachment during the flotation of low rank coal by surface modification. *Int. J. Min. Sci. Technol.* **2020**, *30*, 217–223. [CrossRef]
12. Nasirimoghaddam, S.; Mohebbi, A.; Karimi, M.; Yarahmadi, M.R. Assessment of pH responsive nanoparticles performance on laboratory column flotation cell applying a real ore feed. *Int. J. Min. Sci. Technol.* **2020**, *30*, 197–205. [CrossRef]
13. Wang, L.M.; Yin, S.H.; Wu, A.X. Ore agglomeration behavior and its key controlling factors in heap leaching of low-grade copper minerals. *J. Clean. Prod.* **2021**, *279*, 123705. [CrossRef]
14. Wang, Z.J.; Wu, H.Q.; Xu, Y.B.; Shu, K.Q.; Yang, J.; Luo, L.P.; Xu, L.H. Effect of dissolved fluorite and barite species on the flotation and adsorption behavior of bastnaesite. *Sep. Purif. Technol.* **2020**, *237*, 116387. [CrossRef]

15. Shu, K.Q.; Xu, L.H.; Wu, H.Q.; Xu, Y.B.; Luo, L.P.; Yang, J.; Tang, Z.; Wang, Z.J. In situ adsorption of mixed anionic/cationic collectors in a spodumene–feldspar flotation system: Implications for collector design. *Langmuir* **2020**, *36*, 8086–8099. [CrossRef] [PubMed]

16. Fuerstenau, D.W.; Herrera-Urbina, R.; Mc Glashan, D.W. Studies on the applicability of chelating agents as universal collectors for copper minerals. *Int. J. Miner. Processing* **2000**, *58*, 15–33. [CrossRef]

17. Barzyk, W.; Malysa, K.; Pomianowski, A. The influence of surface oxidation of chalcocite on its floatability and ethyl xanthate sorption. *Int. J. Miner. Processing* **1981**, *8*, 17–29. [CrossRef]

18. Newell, A.; Skinner, W.M.; Bradshaw, D.J. Restoring the floatability of oxidised sulfides using sulfidisation. *Int. J. Miner. Processing* **2007**, *84*, 108–117. [CrossRef]

19. Rashchi, F.; Sui, C.; Finch, J.A. Sphalerite activation and surface Pb ion concentration. *Int. J. Miner. Processing* **2002**, *67*, 43–58. [CrossRef]

20. Gerson, A.R.; Lange, A.G.; Prince, K.E.; Smart, R.S.C. The mechanism of copper activation of sphalerite. *Appl. Surf. Sci.* **1999**, *137*, 207–223. [CrossRef]

21. Finkelstein, N.P. The activation of sulphide minerals for flotation: A review. *Int. J. Miner. Processing* **1997**, *52*, 81–120. [CrossRef]

22. Kartio, I.J.; Basilio, C.I.; Yoon, R.-H. An XPS Study of Sphalerite Activation by Copper. *Langmuir* **1998**, *14*, 5274–5278. [CrossRef]

23. Majima, H. How oxidation affects selective flotation of complex sulphide ores. *Can. Metall. Q.* **1969**, *8*, 269–273. [CrossRef]

24. Hampton, M.A.; Plackowski, C.; Nguyen, A.V. Physical and chemical analysis of elemental sulfur formation during galena surface oxidation. *Langmuir* **2011**, *27*, 4190–4201. [CrossRef] [PubMed]

25. Nowak, P.; Laajalehto, K. Oxidation of galena surface—An XPS study of the formation of sulfoxy species. *Appl. Surf. Sci.* **2000**, *157*, 101–111. [CrossRef]

26. Du, C.H. *Experimental Study on Flotation Separation of Copper-Lead-Zinc Sulfide Mixed Concentrate*; Wuhan University of Technology: Wuhan, China, 2019.

27. Zhou, Y.C. Study on the mineral processing technology of a refractory low grade copper sulfide ore. *Non-Ferr. Min. Metall.* **2013**, *29*, 31–34.

28. Liu, S.; Liu, W.; Sun, Z.; Tian, W.; Wang, L.; Ye, Y.; Zeng, K. Study on ISO-flotation and differential-flotation flow sheet technology of copper-pyrite ore. *China Min. Mag.* **2014**, *23*, 225–234.

29. Wang, Y.J.; Yin, Z.G.; Wang, H.B. Study on differential flotation process for Cu-S ore. *Conserv. Util. Miner. Resour.* **2011**, *3*, 15–18.

30. Xu, H.F.; Zhong, H.; Tang, Q.; Wang, S.; Zhao, G.; Liu, G.Y. A novel collector 2-ethyl-2-hexenoic hydroxamic acid: Flotation performance and adsorption mechanism to ilmenite. *Appl. Surf. Sci.* **2015**, *353*, 882–889. [CrossRef]

31. Nuri, O.S.; Irannajad, M.; Mehdilo, A. Reagent adsorption on modified mineral surfaces: Iso-therm, kinetic and thermodynamic aspects. *J. Mol. Liq.* **2019**, *291*, 111311. [CrossRef]

32. Huang, Z.Q.; Zhong, H.; Wang, S.; Xia, L.Y.; Zou, W.B.; Liu, G.Y. Investigations on reverse cationic flotation of iron ore by using a Gemini surfactant: Ethane-1,2-bis (di-methyl-dodecyl-ammonium bromide). *Chem. Eng. J.* **2014**, *257*, 218–228. [CrossRef]

33. Liu, G.Y.; Zhong, H.; Xia, L.Y.; Wang, S.; Xu, Z.H. Improving copper flotation recovery from a refractory copper porphyry ore by using ethoxycarbonyl thiourea as a collector. *Miner. Eng.* **2011**, *24*, 817–824.

34. Liu, G.Y.; Zeng, H.B.; Lu, Q.Y.; Zhong, H.P.; Choi Xu, Z.H. Adsorption of mercaptobenzoheterocyclic compounds on sulfide mineral surfaces: A density functional theory study of structure–reactivity relations. *Colloids Surf. A Physicochem. Eng. Asp.* **2012**, *409*, 1–9. [CrossRef]

35. Liu, G.Y.; Xiao, J.J.; Zhou, D.W.; Zhong, H.; PChoi Xu, Z.H. A DFT study on the structure-reactivity relationship of thiophosphorus acids as flotation collectors with sulfide minerals: Implication of surface adsorption. *Colloids Surf. A Physicochem. Eng. Asp.* **2013**, *434*, 243–252. [CrossRef]

36. Chen, J.H.; Lan, L.H.; Chen, Y. Computational simulation of adsorption and thermodynamic study of xanthate, dithiophosphate and dithiocarbamate on galena and pyrite surfaces. *Miner. Eng.* **2013**, *46–47*, 136–143. [CrossRef]

37. Baldwin, D.A.; Manton, M.R.; Pratt, J.M.; Storey, M.J. Studies on the flotation of sulphides. I. The effect of Cu(II) ions on the flotation of zinc sulphide. *Int. J. Miner. Processing* **1979**, *6*, 173–192. [CrossRef]

38. Liu, G.Y.; Zhong, H.; Dai, T.G. Separation of chalcopyrite from pyrite at slightly alkaline conditions using ethoxylcarbonyl thionocarbamate as collector. *Chin. J. Nonferrous Met.* **2006**, *16*, 1108–1114.

39. Ding, J. *Study on the Performance of Ionic Nano-Collectors and Its Mechanism of Reaction with Micro Fine Chalcopyrite*; Jiangxi University of Technology: Jiangxi, China, 2018.

40. Zhang, X.Z. *Study of Flotation New Collector in Anhui Copper Mine*; Wuhan University of Technology: Wuhan, China, 2013.

41. Li, T.S. *Study on Application of New Collector in Wushan Copper Mine*; Wuhan University of Technology: Wuhan, China, 2013.

42. Xu, B.; Wu, J.T.; Dong, Z.L.; Jiang, T.; Li, Q.; Yang, Y.B. Flotation performance, structure–activity relationship and adsorption mechanism of a newly-synthesized collector for copper sulfide minerals in Gacun polymetallic ore. *Appl. Surf. Sci.* **2021**, *551*, 149420. [CrossRef]

43. Xu, B. *The Study of the New Flotation Reagent and the New Comprehensive Recovery Process of Tetrahedrite Type Copper-Lead-Zinc Sulfide Ore*; Central South University: Changsha, China, 2013.